Improved thermal and electrical properties of Al-doped $Ge_2Sb_2Te_5$ films for phase-change random access memory

2012 J. Phys. D: Appl. Phys. 45 375302

(http://iopscience.iop.org/0022-3727/45/37/375302)

IOP PUBLISHING JOURNAL OF PHYSICS D: APPLIED PHYSICS

J. Phys. D: Appl. Phys. **45** (2012) 375302 (6pp) doi:10.1088/0022-3727/45/37/375302

Improved thermal and electrical properties of Al-doped $Ge_2Sb_2Te_5$ films for phase-change random access memory

Guoxiang Wang[1,2], Xiang Shen[1], Qiuhua Nie[1,2,5], Rongping Wang[3], Liangcai Wu[4], Yegang Lv[4], Fen Chen[1], Jing Fu[1], Shixun Dai[1] and Jun Li[1]

[1] Faculty of Information Science and Engineering, Ningbo University; Ningbo 315211, People's Republic of China
[2] Shanghai Institute of Technical Physics, Chinese Academy of Sciences, Shanghai 200083, People's Republic of China
[3] Laser Physics Centre, Australian National University, Canberra, ACT 0200, Australia
[4] Shanghai Institute of Micro-system and Information Technology, Chinese Academy of Sciences, Shanghai 200050, People's Republic of China

E-mail: wodehaiyang88@126.com

Received 6 June 2012, in final form 24 July 2012
Published 30 August 2012
Online at stacks.iop.org/JPhysD/45/375302

Abstract

$Al_x(Ge_2Sb_2Te_5)_{100-x}$ materials with different Al contents are systemically studied for applications in phase-change random access memory (PRAM) devices. Al-doped $Ge_2Sb_2Te_5$ (GST) films show better thermal stability than GST because they do not have phase transformation from face-centred cubic (fcc) to hexagonal at high annealing temperatures. As the Al content increases, the resistance in both amorphous and crystalline phases improves and there is four to five orders of magnitude difference in the resistance between the amorphous and crystalline phases, all of which are helpful in achieving a higher On/OFF ratio for PRAM. In addition, the introduction of Al into the GST films can increase the optical band gap that is favourable to decrease the threshold current of PRAM devices. Raman spectra show that a significant change in the local bonding arrangement around Sb atoms has occurred due to the phase transformation from fcc to hexagonal in the GST film but this can be suppressed by Al addition during the crystallization process. All these results confirm that Al-doped GST films are suitable for use in PRAM.

(Some figures may appear in colour only in the online journal)

1. Introduction

Phase-change random access memory (PRAM) using phase-change materials has emerged as a potential candidate for the next-generation non-volatile memory technology. Its performance depends critically on the Joule heating for reversible phase change between amorphous and crystalline phases of chalcogenide materials. For example, the applications in rewritable optical media (CD, DVD, Blu-Ray Disc) and electronic non-volatile memories are based on the strong optical and electronic contrast between the two phases [1]. In recent years, $Ge_2Sb_2Te_5$ (GST) alloys have been proposed for use in PRAM due to their excellent properties with respect to thermal stability, cyclability and crystallization speed [2]. However, with increasing need of low power consumption, good data retention and challenge of reducing the RESET current for PRAM applications [3], the performance of the mostly adopted GST still needs to be improved. In fact, much effort has been made by doping various elements, such as N [4], O [5], Si [6], SiO_2 [7], Bi [8], Ag [9], Sn [10] and so on, into GST in order to modify its material properties for phase-change applications.

According to recent studies [11–13], Al atoms were reported to form covalent bonds with Sb or Te and reduce the

[5] Author to whom any correspondence should be addressed.

Table 1. Chemical composition of the Al-doped GST films using different GST sputtering powers.

Film	GST power (W)	Al power (W)	Al (at%)	Ge (at%)	Sb (at%)	Te (%)	d(nm)
$Ge_2Sb_2Te_5$	25	0	0	21.56	23.70	54.74	350
$Al_{14.43}(GST)_{85.57}$	75	15	14.43	23.31	19.32	42.94	330
$Al_{21.73}(GST)_{78.27}$	50	15	21.73	19.66	18.32	40.28	320
$Al_{23.19}(GST)_{76.81}$	40	15	23.19	16.57	18.60	41.64	350

atomic diffusivity, which could provide sufficient amorphous stability for phase-change films. If Al atoms can also form covalent bonds with Sb or Te in Al-doped GST, the stability of GST will significantly be improved. In fact, this has been confirmed in [14], which reported that Al doped into a GST film restricted the fcc-to-hexagonal transition and increased the crystallization temperature (T_c) from amorphous to the fcc phases. However, contradictory results in [15] show that Al doping did not cause an increase in the T_c of GST films. Therefore, further investigation on the structure and various physical properties is necessary to elucidate the role of Al doping in GST materials.

In this paper, $Al_x(Ge_2Sb_2Te_5)_{100-x}$ ($x = 14.43$, 21.73, 23.19 at%) films were prepared by the magnetron co-sputtering method. The effect of Al doping on the crystallization behaviours, and structural, thermal, optical and electrical properties of GST phase-change films were investigated systematically with the help of x-ray diffraction, Raman spectra, UV–VIS–NIR spectrophotometry and sheet resistance versus temperature (R–T).

2. Experimental

Al-doped GST films were deposited on quartz substrates with size 2 cm × 2 cm by the magnetron co-sputtering method using separate Al and GST alloy targets, and the base and working pressures were set to be 1.8×10^{-4} Pa and 0.2 Pa, respectively. The dc power on the Al target of 50 mm diameter was fixed to be 15 W, while the RF power on the GST target of 50 mm diameter was tuned in a range from 25 to 75 W in order to obtain the different Al doping content. Meanwhile, GST thin films were also prepared for comparison.

The compositions of the as-deposited films, measured by energy dispersive spectroscopy (EDS), are listed in table 1. The structures of the as-deposited and annealed thin films were examined by the x-ray diffraction technique (Bruker D2 PHASER diffractometer). The sheet resistance of the as-deposited film as a function of the elevated temperature (non-isothermal) was *in situ* measured using a four-point probe in a homemade vacuum chamber. The optical transmittance (T_{op}) in the spectral range 300–2500 nm was obtained by a Perkin-Elmer Lambda 950 UV–VIS–NIR spectrophotometer. The absorption coefficient (α) was calculated using the general relation $\alpha = -(1/d)\ln(T_{op})$, where d is the thickness of the film measured by the surface profiler and listed in table 1. The optical band gap (E_{opt}) was also evaluated using the absorption properties, which were expressed as $\alpha(v) \cdot hv = B(hv - E_{opt})^2$, where hv is the energy of the incident photon and B is a parameter that depends on the electronic transition probability. Raman scattering spectroscopy was recorded at room temperature using a backscattering configuration. An Ar ion laser with a wavelength of 785 nm was used as an excitation source. The power density on the sample was kept at low levels (~0.2 mW μm^{-2}) in order to avoid any structural deformation induced by laser radiation.

3. Results and discussion

Figure 1(*a*) shows the XRD patterns of the undoped and Al-doped GST films. No diffraction peaks were observed, indicating the amorphous nature of all the as-deposited films. However, while the films were annealed at 200 °C, a set of diffraction patterns corresponding to a NaCl-type face-centred cubic (fcc) structure appeared, as shown in figure 1(*b*). Moreover, it was also found that the diffraction intensity in the Al-doped GST films was weak compared with that in the undoped GST film, indicating that Al could suppress the growth of crystalline gains in the films resulting in the decrease in the diffraction intensity peaks, as shown in figure 1(*b*). The smaller grain size may induce more grain boundaries and more carrier scattering [16, 17], leading to an increase in the crystalline resistance of the Al-doped GST films and a decrease in the power consumption of the cell device.

If the annealing temperature is further increased to 400 °C, the undoped GST film is dominated by the hexagonal phase, as shown in figure 1(*c*). It is also interesting to see that the hexagonal phase begins to disappear in the Al-doped GST films and only the hexagonal-(1 0 3) peak still exists in the crystalline $Al_{14.43}(GST)_{85.57}$ film. With a further increase in Al dopant, both $Al_{21.73}(GST)_{78.27}$ and $Al_{23.19}(GST)_{76.81}$ films are entirely dominated by the fcc phase, indicating that the Al atoms can suppress the fcc-to-hexagonal phase transition.

Thermal stability in the amorphous state is one of the important parameters that determines the performance of data retention in PRAM devices. Figure 2 shows the temperature dependence of the sheet resistance R_s at a heating rate of 50 K min^{-1}. With increase in temperature, a continuous decrease in resistance is observed for all the films, and then an abrupt drop in resistance occurs when the temperature reaches their respective crystallization temperature (T_c) for the undoped and Al-doped GST films. The obtained crystallization temperature increases with increasing Al concentration, being ~170 °C, ~177 °C, ~208 °C and ~220 °C for GST, $Al_{14.43}(GST)_{85.57}$, $Al_{21.73}(GST)_{78.27}$ and $Al_{23.19}(GST)_{76.81}$, respectively. The increase in crystallization temperature could be due to the unique role of Al in the films, e.g. Al atoms in the films reduce the density of dangling bonds available for re-engagement during crystallization, which finally could improve the archival life stability of PRAM devices [18].

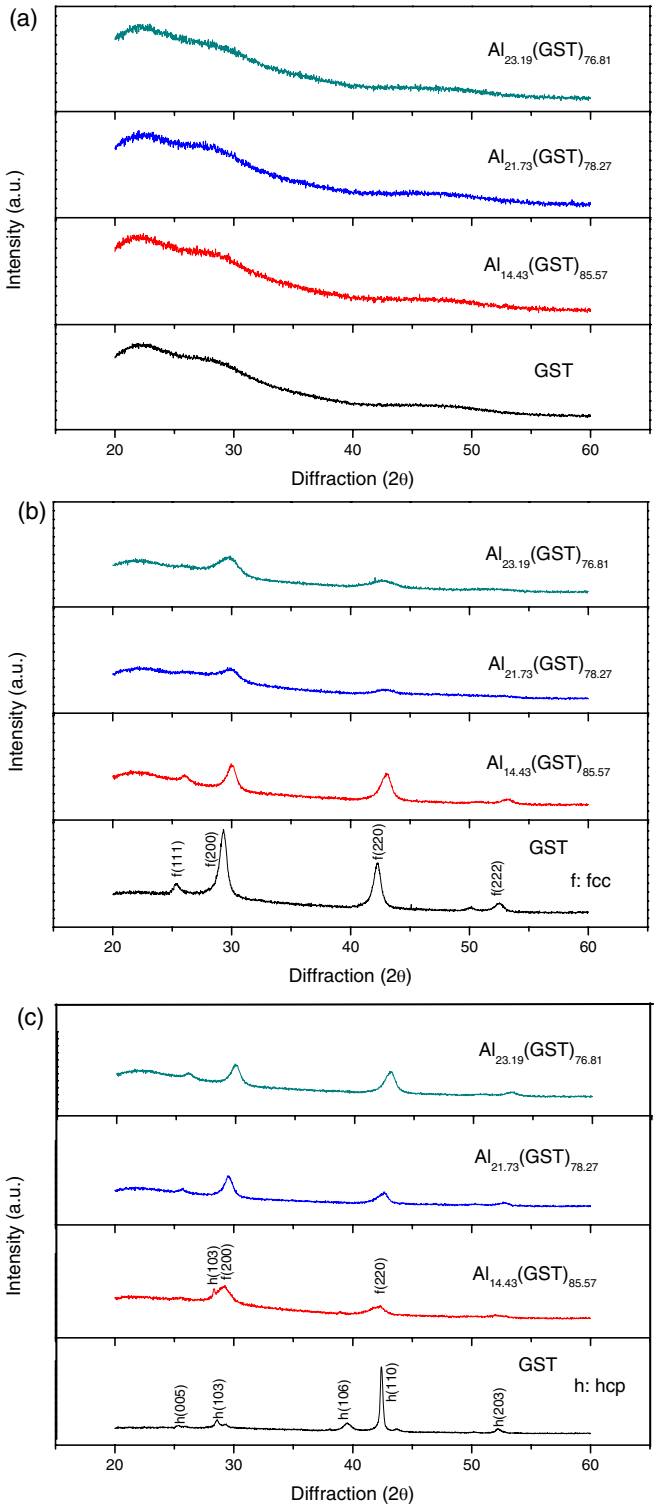

Figure 1. XRD patterns of (*a*) as-deposited undoped and Al-doped GST, (*b*) 200 °C-annealed undoped and Al-doped GST, (*c*) 400 °C-annealed undoped and Al-doped GST.

It is worthwhile to note that the undoped GST film exhibits another transition at ∼280 °C that corresponds to the fcc-to-hexagonal phase transition, which has not appeared in Al-doped GST films, as shown in figure 2. This is consistent with the results of XRD analysis. On the other hand, the

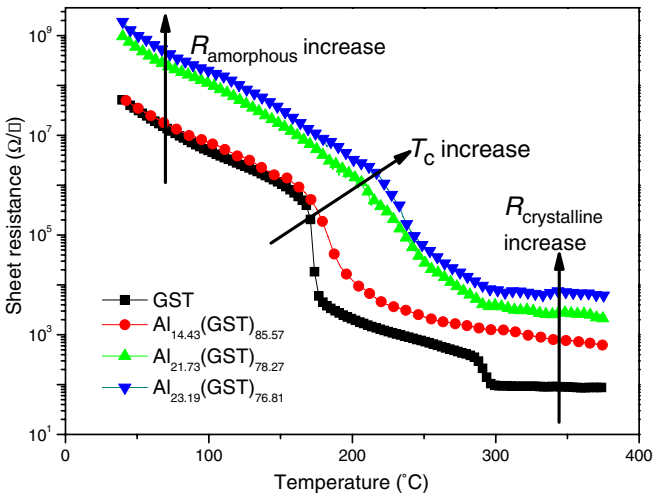

Figure 2. Temperature dependence of the sheet resistance R_s of the GST and Al-doped GST films at a heating rate of 50 K min^{-1}.

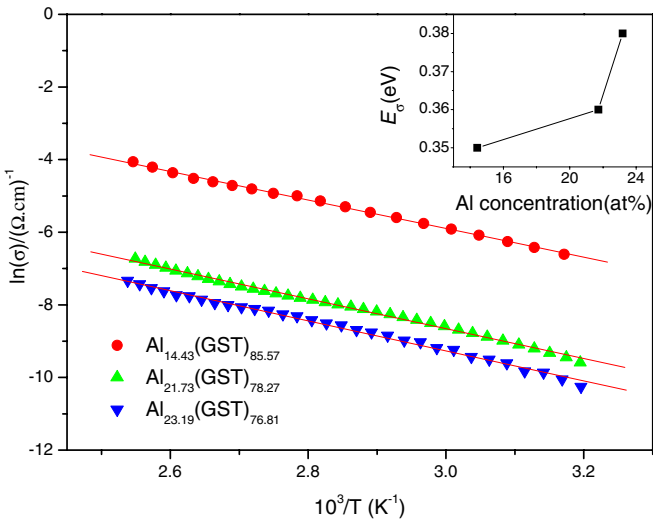

Figure 3. Dependence of electrical conductivity on the reciprocal temperature for amorphous Al-doped GST films; up-right inset figure is dependence of electrical conduction activation energy on the Al concentration.

Al-doped GST films exhibit a higher sheet resistance in both amorphous and crystalline phases compared with the undoped GST film. There is four to five orders of magnitude difference between the amorphous and crystalline phases. This may lead to a lower power consumption of PRAM devices and is helpful in achieving a higher On/OFF ratio [19].

Figure 3 shows the conductivity (s) of the amorphous films as a function of the reciprocal temperature in the range 38–120 °C for the Al-doped GST films. A similar linear relationship between the conductivity and temperature suggests that all the films follow the same conductivity, where the contribution from thermal activation of carriers in the films is dominant. In fact, such a mechanism has been found in other amorphous chalcogenide materials, where the conductivity can be expressed by an Arrhenius-type relation [20]:

$$\sigma = \sigma_0 \exp\left(-\frac{E_\sigma}{k_B T}\right), \quad (1)$$

where σ_0 is a pre-exponential factor depending on the composition of the films, E_σ is the electrical conduction activation energy, k_B is the Boltzmann constant and T is the absolute temperature. From the plot of ln σ versus $10^3/T$, the electrical conduction activation energy (E_σ) can be calculated from the slope (E_σ/k_B) of the plot. The obtained values of E_σ are plotted as a function of the dopant concentration, as shown in the inset of figure 3. The activation energies for electrical conduction E_σ of GST, $Al_{14.43}(GST)_{85.57}$, $Al_{21.73}(GST)_{78.27}$ and $Al_{23.19}(GST)_{76.81}$ are ~0.35 eV [21], ~0.35 eV, ~0.36 eV and ~0.38 eV, respectively.

The electrical conduction activation energy also has a simple relation with the band gap [22]:

$$E_\sigma = E_g/2 + \Delta E, \quad (2)$$

where $E_g/2$ is the distance from the Fermi level to the conduction band and ΔE is the depth of the trap states. In the case of intrinsic conduction with equal number of electrons and holes, the Fermi level is situated in the middle of the band gap. Thus, we can roughly estimate the optical band gaps of amorphous GST, $Al_{14.43}(GST)_{85.57}$, $Al_{21.73}(GST)_{78.27}$ and $Al_{23.19}(GST)_{76.81}$ to be ~0.70 eV, ~0.70 eV, ~0.72 eV and ~0.76 eV, respectively. The band gap value of amorphous GST is in good agreement with the experimental result, ~0.697 eV, measured by optical spectroscopy (see figure 4).

Figure 4(a) shows the plots of $(\alpha(v)hv)^{1/2}$ versus hv for the amorphous and polycrystalline (annealed at 200 and 400 °C) GST films. The investigations show that the transmission of GST films becomes extremely low (see the inset of figure 4(a)) and the optical band gap is decreased continuously after the amorphous–crystalline transformation. Figure 4(b) shows changes in the optical band gap of the GST and Al-doped GST films as a function of the annealing temperature. The optical band gap increases with increasing Al incorporation for the as-deposited films. This could be due to the fact that the as-deposited amorphous thin films always contain a high concentration of unsaturated bonds or defects that account for the presence of localized states in the amorphous band gap. The incorporation of Al could reduce the number of unsaturated bonds, and thus decrease the density of localized states in the band structure and consequently increase the optical band gap. The large band gap is favourable to decrease the threshold current of PRAM devices [23].

When the Al-doped GST films are crystallized from an amorphous state to a NaCl-type fcc structure, their band gaps are decreased first and then keep slightly changing even when the annealing temperature goes up to 400 °C. However, for the undoped GST film annealed at 400 °C, the optical band gap further decreases due to the formation of a hexagonal structure.

Figures 5(a), (b) and (c) show the Raman spectra of the as-deposited, 200 °C-annealed and 400 °C-annealed undoped and Al-doped GST films, respectively. We have carefully used appropriate measurement parameters to avoid any structural modification of the GST layers by the laser beam, and achieved the spectra with good signal-to-noise ratio that are in contrast with those in [24–27]. Basically, the Raman spectra consist of these features: (1) for the as-deposited undoped GST films, the Raman spectra are dominated by a broad band covering

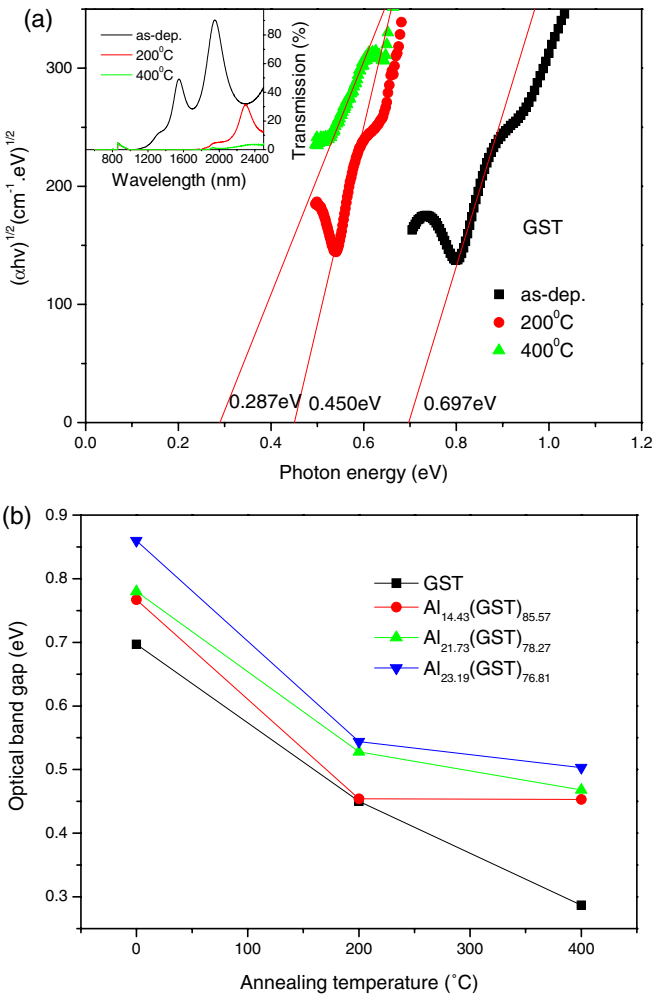

Figure 4. (a) Plots of $(\alpha hv)^{1/2}$ versus hv for the GST films; up-left inset figure is the corresponding Vis–IR transmission spectra. (b) Changes in the optical band gap of GST and Al-doped GST films as functions of the amount of incorporated Al and annealing temperature.

the region 100–190 cm^{-1}. Two broad peaks overlap with each other in this region with one peak at 125 cm^{-1} (peak A) and another at 150 cm^{-1} (peak B). Peak A is associated with the A_1 mode of $GeTe_{4-n}Ge_n$ (n = 0,1,2) tetrahedral modes [28], while peak B is related to Sb–Te bonds' vibrations in the $Sb–Te_3$ units [29]. In addition, a weak and broad Raman band is located at ~220 cm^{-1} (peak C), assigned to the F_2 mode of $GeTe_4$ tetrahedra [30]. In the low-frequency region of the spectra, a peak at ~56 cm^{-1} (peak D) can be observed, which is related to the E mode of $GeTe_4$ tetrahedra [30]. All Al-doped GST films exhibit similar Raman spectra in terms of peak position. However, the intensity of the peak at 150 cm^{-1} decreases with increasing Al content, suggesting that the addition of Al leads to a higher degree of disorder in the amorphous phase of the material. In fact, this is in agreement with the high crystallization temperature of the Al-doped GST film. In fact, the higher the disorder level of the Al-doped GST amorphous state, the higher the energy required to arrange it in an ordered crystalline form [31]. (2) For the films annealed at 200 °C, the broadening nature of the Raman spectrum is still preserved, as shown in figure 5(b), but the peaks at ~125 cm^{-1}

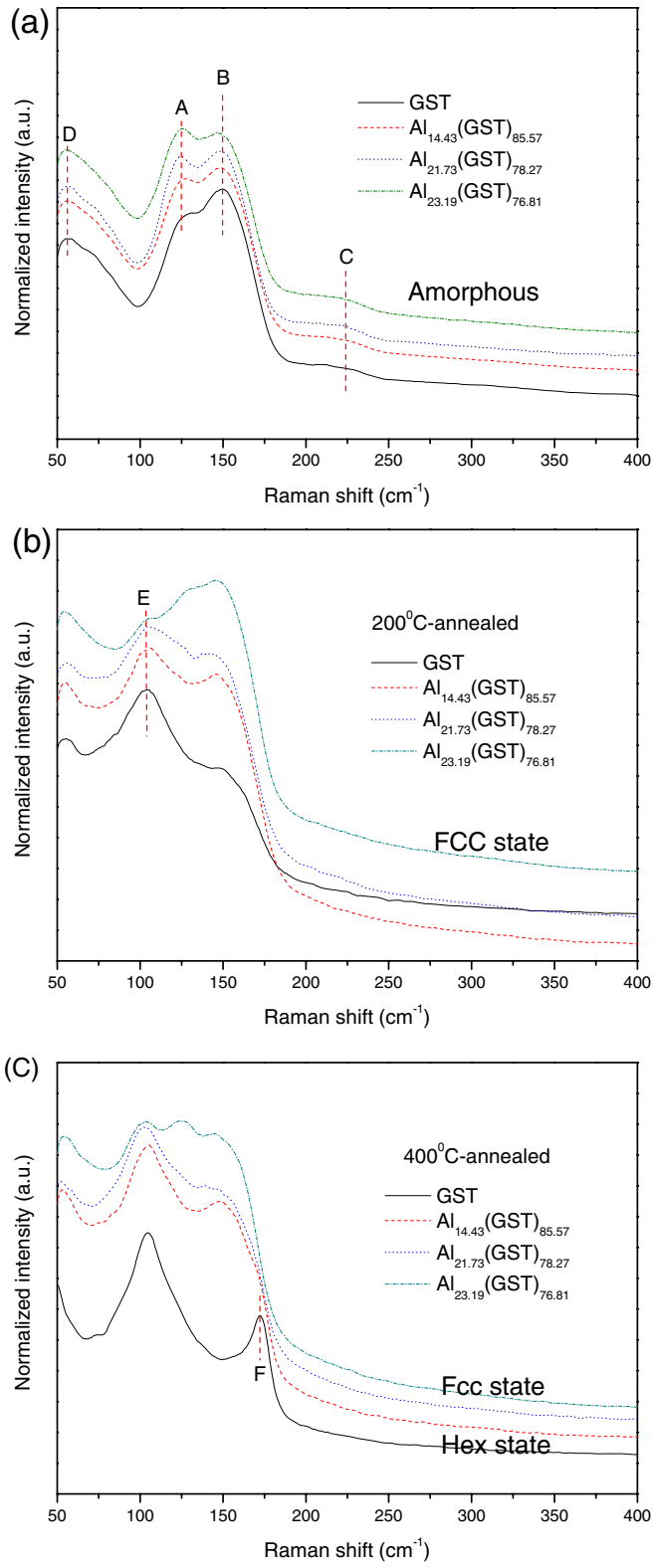

Figure 5. Raman scattering spectra of (*a*) as-deposited undoped and Al-doped GST, (*c*) 200 °C-annealed undoped and Al-doped GST, (*d*) 400 °C-annealed undoped and Al-doped GST.

(peak A) and ∼220 cm^{-1} (peak C) in figure 5(*a*) disappear (or they are at least suppressed) due to the annealing-induced crystallization. Instead, a new peak at ∼105 cm^{-1}(peak E) appears that is related to the A_1 mode of $GeTe_4$ corner-sharing tetrahedra [32]. The results reveal that the GeTe component of GST alloys is mainly responsible for the phase transition [32]. On the other hand, although there is a change in the intensity of peak B at 150 cm^{-1} in figure 2(*b*), its position seems not to be significantly influenced by the crystallization process, which is in good agreement with the general consensus about unchanged local arrangement of atoms around Sb on crystallization [33]. (3) For the films annealed at 400 °C, Peak E at 105 cm^{-1} remains almost unchanged while peak B at 150 cm^{-1} disappears and a new sharp peak F at ∼172 cm^{-1} appears in the undoped GST film annealed at 400 °C, as shown in figure 5(*c*). It may be assigned to Te–Te pairs, similar to glasses in the Ge–Se–Te system [34]. In our opinion, the evaluation of the peak still needs further investigation. The new peak F cannot be observed in the Al-doped GST films. This reveals that a significant change in the local bonding arrangement around Sb atoms has occurred in the GST film but the phenomenon can be restrained by Al addition due to the suppression of phase transformation from fcc to hexagonal. This is qualitatively confirmed by the Raman spectra shown in this work.

More interestingly, if we compare the Raman spectra of the as-deposited and annealed $Al_{23.19}(GST)_{76.81}$ films, the peaks at ∼125 and ∼150 cm^{-1} exist in all cases. We argue that these characterizations reveal that the structure of the film can be stabilized with proper Al dopant.

4. Conclusions

In this paper, the structural, optical and electrical properties of $Al_x(Ge_2Sb_2Te_5)_{100-x}$ (x = 14.43, 21.73, 23.19 at%) films compared with the GST film are studied systematically. Adding aluminium into the GST film tends to foster a very stable one-step phase transition from amorphous → face-centred cubic (fcc). With increasing Al content, the $Al_x(GST)_{100-x}$ films possess a larger set/reset resistance and wider band gap, which is advantageous to decrease the threshold current in the related PRAM devices. On the other hand, the Al-rich GST films also exhibit a higher crystallization temperature and enhanced the thermal stability of amorphous phase and ensure good data retention ability. Raman spectra of the thin films suggest that the local bonding arrangement around Ge atoms changes and that around Sb atoms is preserved due to the Al addition even at a high annealing temperature of 400 °C. All these results confirm that Al-doped GST films have huge potential applications in future PRAM devices.

Acknowledgments

This work was financially supported by the International Science and Technology Cooperation Program of China (Grant No 2011DFA12040), the National Program on Key Basic Research Project (973 Program) (Grant No 2012CB722703), the Natural Science Foundation of China (Grant Nos 61008041 and 60978058), the Natural Science Foundation of Zhejiang Province, China (Grant Nos Y1090996 and R1101263), the Program for New Century Excellent Talents in

University (Grant No NCET-10-0976), the Scientific Research Fund of Zhejiang Provincial Education Department (Grant Nos Y200907452 and Y200803996), the Natural Science Foundation of Ningbo City, China (Grant No 2011A610092), the Program for Innovative Research Team of Ningbo city (Grant No 2009B21007), and sponsored by the K C Wong Magna Fund in Ningbo University.

References

[1] Wuttig M and Yamada N 2007 *Nature Mater.* **6** 824
[2] Yamada N, Ohno E, Nishiuchi K and Akahira N 1991 *J. Appl. Phys.* **69** 2849
[3] Lee M L, Yong K T, Gan C L and Ting L H 2008 *J. Phys. D: Appl. Phys.* **41** 215402
[4] Jeong T H, Kim M R, Seo H, Park J W and Yeon C 2000 *Japan. J. Appl. Phys.* **39** 2775
[5] Privitera S, Rimini E and Zonca R 2004 *Appl. Phys. Lett.* **85** 3044
[6] Feng J, Zhang Y, Qiao B W, Lai Y F, Lin Y Y and Cai B C 2007 *Appl. Phys.* A **87** 57
[7] Ryu S W, Oh J H and Lee J H 2008 *Appl. Phys. Lett.* **92** 142110
[8] Wang K, Wamwangi D, Ziegler S, Steimer C and Wuttig M 2004 *J. Appl. Phys.* **96** 5557
[9] Song K H, Kim S W, Seo J H and Lee H Y 2009 *Thin Solid Films* **517** 3958
[10] Kojima R and Yamada N 2001 *Japan. J. Appl. Phys.* **40** 5930
[11] Peng C, Wu L C, Song Z T, Rao F and Zhu M 2011 *Appl. Phys. Lett.* **99** 043105
[12] Run K, Rao F, Song Z T, Lv S L and Cheng Y 2012 *Appl. Phys. Lett.* **100** 052105
[13] Peng C, Wu L C, Song Z T, Rao F and Zhu M 2011 *Appl. Surf. Sci.* **257** 10667
[14] Wei S J, Li J, Wu X, Zhou P, Wang S Y and Zheng Y X 2007 *Opt. Express* **15** 10584
[15] Seo J H, Song K H and Lee H Y 2010 *J. Appl. Phys.* **108** 064515
[16] Wei S J, Zhu H F, Chen K, Xu D, Li J and Gan F X 2011 *Appl. Phys. Lett.* **98** 231910
[17] Gu Y F, Cheng Y, Song S N, Zhang T and Song Z T 2011 *Scr. Mater.* **65** 622
[18] Cao K, Ferizovic D and Munoz M 2008 *J. Appl. Phys.* **104** 123511
[19] Wang C Z, Li S M, Zhai J W and Shen B 2011 *Scr. Mater.* **64** 645
[20] Chung K, Wamwangi D, Woda M, Wuttig M and Bensch W 2008 *J. Appl. Phys.* **103** 083523
[21] Rao F, Song Z T, Ren K, Zhou X L, Cheng Y, Wu L C and Liu B 2011 *Nanotechnology* **22** 145702
[22] Gu Y F, Song S N, Song Z T, Cheng Y and Du X F 2012 *J. Appl. Phys.* **111** 054319
[23] Welnic W, Pamungka A, Delemple R, Steimer C, Blugel S and Wutting M 2006 *Nature. Mater.* **5** 56
[24] Tominaga J and Atoda N 1999 *Japan. J. Appl. Phys. Part 2* **38** L322
[25] Zhang G J, Gu D H, Gan F X, Sun Z R and Guo J Y 2004 *Chin. Opt. Lett.* **2** 555
[26] Satoh H, Sugawara K and Tanaka K 2006 *J. Appl. Phys.* **99** 024306
[27] Zhang G J, Gu D H, Jiang X W, Chen Q X and Gan F X 2006 *Appl. Surf. Sci.* **252** 4083
[28] Nemec P, Moreac A, Nazabal V, Pavlista M, Prikryl J and Frumar M 2009 *J. Appl. Phys.* **106** 103509
[29] Watanabe I, Noguchi S and Shimizu T 1983 *J. Non-Cryst. Solids* **58** 35
[30] Andrikopoulos K S, Yannopoulous S N, Voyiatzis G A, Kolobov A V, Ribes M and Tominaga J 2006 *J. Phys.: Condens. Matter* **18** 965
[31] Betti Beneventi G, Perniola L, Sousa V, Gourvest E, Maitrejean S and Bastien J C 2011 *Solid State Electron.* **65–66** 197
[32] Kolobov A N, Fons P and Tominaga J 2007 *Thin Solid Films* **515** 7534
[33] Kolobov A V, Fons P, Frenkel A I, Ankudinov A L, Tominaga J and Uruga T 2004 *Nature. Mater.* **3** 703
[34] Moharram A H, Hefni M A and Abdel-Baset A M 2010 *J. Appl. Phys.* **108** 073505